 CMES, vol.99, no.6, pp.491-508, 2014

3D Echo-Based Patient-Specific Computational Left Ventricle Models to Quantify Material Properties and Stress/Strain Differences between Ventricles with and without Infarct

Rui Fan[1], Dalin Tang[2,3], Jing Yao[4], Chun Yang[5] and Di Xu[4]

Abstract: Identifying ventricle material properties and its infarct area after heart attack noninvasively is of great important in clinical applications. An echo-based computational modeling approach was proposed to investigate left ventricle (LV) mechanical properties and stress conditions using patient-specific data. Echo data was acquired from one healthy volunteer (male, age: 58) and a male patient (age: 60) who had an acute inferior myocardial infarction one week before echo image acquisition. Standard echocardiograms were obtained using an ultrasound machine (E9, GE Mechanical Systems, Milwaukee, Wisconsin) with a 3V probe and data were segmented for model construction. Finite element models were constructed to obtain ventricle stress and strain conditions. A pre-shrink process was applied so that the model ventricle geometries under end-of-systole pressure matched in vivo data. Our results indicated that the modeling approach has the potential to be used to determine ventricle material properties. The equivalent Young's modulus value from the healthy LV (LV1) was about 30% softer than that of the infarct LV (LV2) at end of diastole, but was about 100% stiffer than that of LV2 at end of systole. This can be explained as LV1 has more active contraction reflected by stiffness variations. Using averaged values, at end-systole, longitudinal curvature from LV2 was 164% higher than that from LV1. LV stress from LV2 was 82% higher than that from LV1. At end-diastole, L-curvature from LV2 was still 132% higher than that from LV1, while LV stress from LV2 was only 9% higher than that from LV1. Longitudinal curvature and stress showed the largest differences between the two

[1] School of Information and Communication Engineering, Beijing University of Posts and Telecommunications, Beijing, China.

[2] Corresponding author. School of Biological Sciences and Medical Engineering, Southeast University, Nanjing, China.

[3] Mathematical Sciences Department, Worcester Polytechnic Institute, MA 01609 USA.

[4] Department of Cardiology, First Affiliated Hospital of Nanjing Medical University, Nanjing 210029, China.

[5] China United Network Communications Co., Ltd., Beijing, China.

ventricles, with the LV with infarct having higher longitudinal curvature and stress values. Large scale studies are needed to further confirm our findings.

Keywords: Heart attack, infarct, ventricle model, ventricle mechanics, left ventricle.

1 Introduction

Medical images and computational modeling have been used more and more in cardiovascular research with the current trend to develop quantitative methods for personalized medicine [Desmond-Hellmann et al. (2011)]. Accurate and reproducible evaluation of global and regional left ventricular (LV) function is of vital importance for the determination of diagnosis, prognosis, and therapeutic options of multiple cardiovascular diseases. Echocardiography is the main imaging modality for the assessment of left ventricular (LV) structure and function [Sabia et al. (1991); Emond et al., (1994); Quinones et al. (2000); Moller et al. (2006); Thune et al. (2006)]. However, in daily clinical practice echocardiographic evaluation of regional LV function is mainly performed by visual estimation on two-dimensional echocardiographic images, which is known to be subjective and not very reliable [Gopal et al. (1995); Mondelli et al. (2001)]. In addition, it is believed that mechanical forces play an important role in cardiovascular disease development. Quantitative image and mechanical stress/strain analysis may provide useful information for disease diagnosis and treatment recommendations [Tang et al. (2010a); Tang et al. (2010b)].

In the past decade, echocardiographic imaging techniques for quantitatively evaluation of cardiac motion pattern were produced. Doppler tissue imaging, which permits direct interrogation of myocardial deformation, was first applied to assess regional wall deformation [Urheim et al. (2000); Edvardsen et al. (2002)]. Nonetheless, owing to the use of the Doppler effect, angle dependency, noise artifacts, confounding of interpretation by tethering of adjacent myocardium and cardiac translational movements, and assessment being confined to myocardial segments that move along the direction of the ultrasound beam have limited its application [Sutherland et al. (2004)]. Speckle tracking imaging (STI), which is based on tracking of speckle patterns created by interference of ultrasound beams in the myocardium, has been available to assess regional myocardial deformation. It is conceptually angle independent of the ultrasound beam, and can provide for measurement of 3 deformation components (longitudinal, circumferential, and radial) strain [Langeland et al. (2005); Amundsen et al. (2006); Reant et al. (2008)]. However, the inherent limitation of this methodology is its 2D nature which limits its ability to track motion occurring within the imaging plane, while motion

in and out of plane can only be detected as features appearing and disappearing from the image, resulting in noise and interfering with tracking [Seo et al. (2009); Y15]. Recently, 3D STI emerges as the newest technique which is conceptually more accurate in assessment of LV motion pattern by resolving the problem of out-of-plane. Nonetheless, the reproducibility and sensibility of 3D STI system commercially available still require are far from being acceptable. Therefore more accurate construct method is needed clinically.

Recent advances in computational modeling, methods and computer technology have made it possible for computer-simulated procedures to be used in clinical decision-making process to replace empirical and often risky clinical experimentation to examine the efficiency and suitability of various reconstructive procedures in diseased hearts. Peskin pioneered heart modeling effort with his celebrated immersed boundary method [Peskin (1977); Peskin (1989)]. Early MRI-based ventricle models were introduced by Axel and Saber et al. for mechanical analysis and investigations [Axel (2002); Saber et al. (2001)] More recently, Hunter, McCulloch, Guccione, Kerckhoffs, Costa, and many other authors have made great contributions to passive and active ventricle modeling, including the Physiome Project and the Continuity package [McCulloch et al. (1992, 2013); Kerckhoffs et al. (2007); Hunter et al. (2003); Nash and Hunter (2000); Costa et al. (1999); Guccione et al. (1993)]. In our previous papers, patient-specific CMR-based computational RV/LV models with fluid-structure interactions were introduced to assess outcomes of various RV reconstruction techniques with different scar tissue trimming and patch sizes [Tang et al. (2008, 2010a, 2010b, 2011)]. A recent review can be found in Tang et al. (2010b).

In this paper, echo-based 3D LV models were introduced to investigate morphological and mechanical stress/strain differences between ventricle with and without infarct. This will serve as a starting point to use computational models for infarct differentiation and surgical planning.

2 Methods

2.1 3D echo data acquisition

Two subjects were chosen in our study. One is a healthy volunteer, male, 58 years old. The other is a male patient, 60 years old, who had an acute inferior myocardial infarction one week before echo image acquisition. Patient data are given in Table 1.

Standard echocardiograms were obtained using an ultrasound machine (E9, GE Mechanical Systems, Milwaukee, Wisconsin) with a 3V probe. Patients were examined in the left lateral decubitus position, and images were acquired at end ex-

piration in order to minimize global cardiac movement. Apical full-volume 4D acquisitions were obtained. Multi-slice function was activated which enables simultaneous display of equidistant nine short axis views generated from the apical full-volume 4D acquisition. Microsoft Visio (Microsoft Corporation) was used for tracing the endocardium and epicardium in each short axis view of LV and contours were used for model construction. Figures 1 and 2 show the echo images, segmented contours and re-constructed 3D LV geometries from the two patients. The location of infarction was defined as a decrease in or cessation of myocardial contractility, which was determined by two experienced observers through visualization of all LV wall segments.

Table 1: Patient data and ventricle volume data.

	P1 (healthy)		P2 (infarct)	
Age	58		60	
Sex	Male		Male	
Disease	none		inferior myocardial infarction	
Pressure(mmHg)	Min=10	Max=120	Min=10	Max=145
Echo Vol (ml)	Min=43	Max=110	Min=72	Max=138
Echo EF	60.91%		47.83%	
Model Vol (ml)	42.99	110.15	72.4	137.66
Adina Model EF		60.97%		47.67%

2.2 Two-layer anisotropic LV model construction with fiber orientations.

The ventricle material was assumed to be hyperelastic, anisotropic, nearly-incompressible and homogeneous. Infarct tissue was assumed to be hyperelastic, isotropic, nearly-incompressible and homogeneous. The governing equations for the LV model were [Tang et al., 2010a,2010b]:

$$\rho v_{i,tt} = \sigma_{ij,j}, \quad i,j = 1,2,3; \quad \text{sum over j}, \tag{1}$$

$$\varepsilon_{ij} = (v_{i,j} + v_{j,i} + v_{\alpha,i} v_{\alpha,j})/2, \quad i,j,\alpha = 1,2,3, \tag{2}$$

where σ is the stress tensor, ε is the strain tensor, $\mathbf{v}$ is displacement, and ρ is material density. The normal stress was assumed to be zero on the outer LV surface and equal to the pressure conditions imposed on the inner LV surface. Structure-only LV model was used to save model construction effort and computing time. This was adequate for our purpose in this paper to obtain LV stress/strain values for analysis.

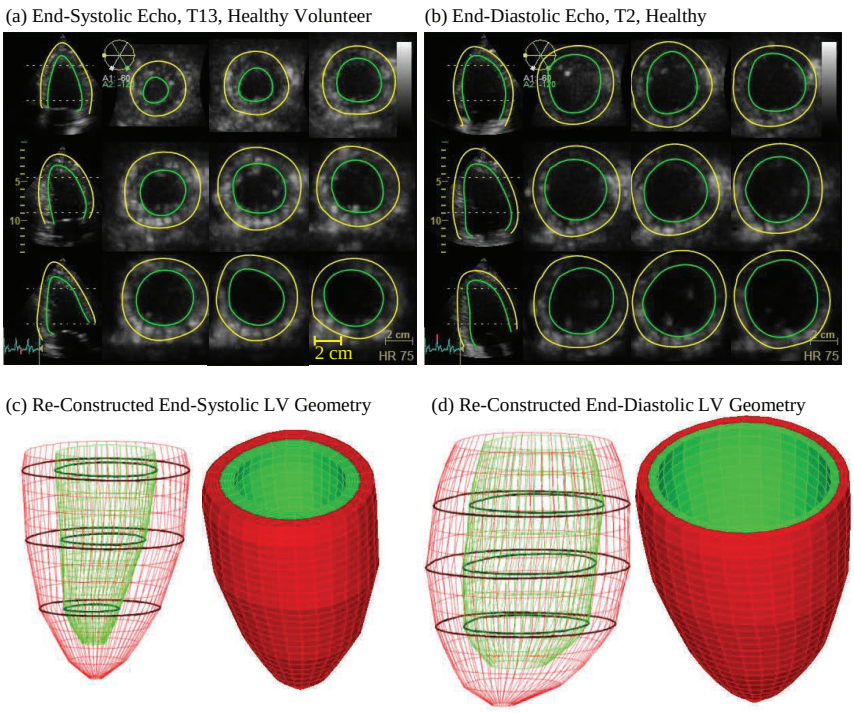

Figure 1: Echo image of a healthy volunteer, contour and re-constructed geometries.

The nonlinear Mooney-Rivlin model was used to describe the nonlinear anisotropic and isotropic material properties. The strain energy function for the isotropic modified Mooney-Rivlin model is given by [Tang et al. (2008,2010a,2010b)]:

$$W = c_1(I_1 - 3) + c_2(I_2 - 3) + D_1[exp(D_2(I_1 - 3)) - 1], \tag{3}$$

where I_1 and I_2 are the first and second strain invariants given by,

$$I_1 = \sum C_{ii}, \quad I_2 = 1/2\left[I_1^2 - C_{ij}C_{ij}\right] \tag{4}$$

$C = [C_{ij}] = X^T X$ is the right Cauchy-Green deformation tensor, $X = [X_{ij}] = [\partial x_i / \partial a_j]$, (x_i) is the current position, (a_i) is the original position, c_i and D_i are material parameters chosen to match experimental measurements [Tang et al. (2010); Humphrey et

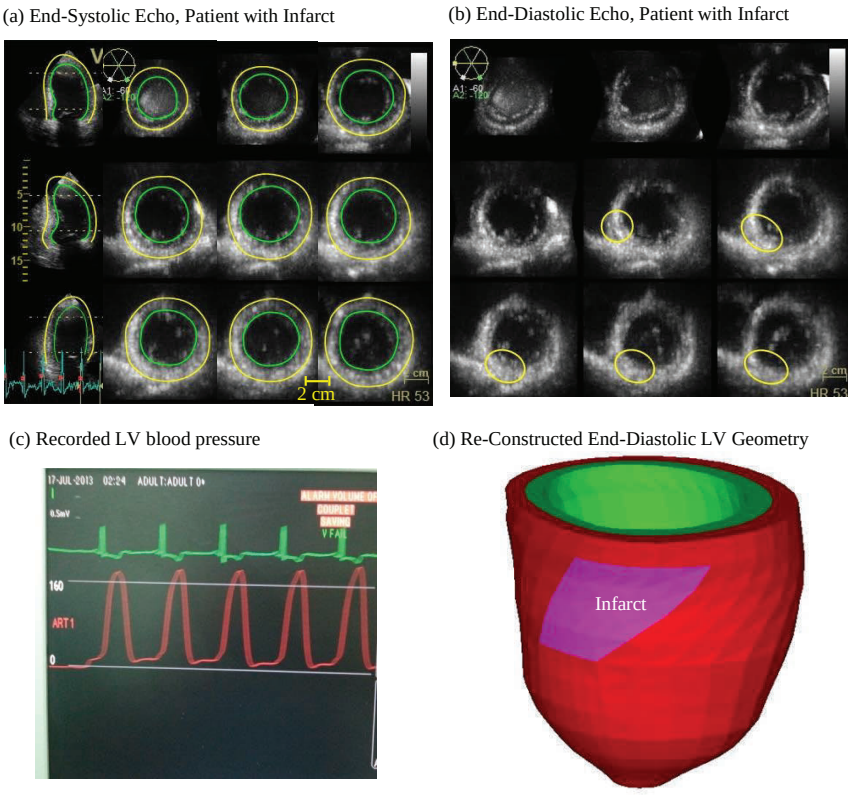

Figure 2: Echo image from a patient with infarct, segmented contours, recorded LV blood pressure profile, and re-constructed geometry. Infarct locations were marked by circles on the echo images.

al. (1990, 2002); Novak et al. (1994)]. The strain energy function for the anisotropic modified Mooney-Rivlin model anisotropic model was obtained by adding an additional anisotropic term in Eq. (3) [Tang et al., (2008,2011)]:

$$W=c_1(I_1-3)+c_2(I_2-3)+D_1[exp(D_2(I_1-3))-1]+K_1/(2K_2)exp[K_2(I_4-1)^2-1], \tag{5}$$

where I_4= C_{ij} $(\mathbf{n}_f)_i$ $(\mathbf{n}_f)_j$, C_{ij} is the Cauchy-Green deformation tensor, $\mathbf{n}_f$ is the fiber direction, K_1 and K_2 are material constants [19]. A two-step least-squares method was used to determine the parameter values in Eq. (5) to fit the experimental data [McCulloch et al. (1992)]. Choosing c_1=0.351 kPa, c_2=0, D_1=0.0633 kPa, D_2 =5.3, K_1=1.913 kPa, K_2 =6.00, it was shown in atng et al. (2011) that stress-

strain curves derived from Eq. (5) agreed well with the stress-strain curves from the dog model given in McCulloch et al. (1992). Parameter values were then adjusted to fit echo-measured LV volume data. The stress-stretch curves and parameter values of the LV and infarct tissues are reported in next section.

As patient-specific fiber orientation data was not available from these patients, we chose to construct a two-layer RV/LV model and set fiber orientation angles using fiber angles given in Hunter et al. (2003). Fiber orientation can be adjusted when patient-specific data becomes available [Sanchez-Quintana, Anderson and Ho, (1996)]. Figure 3 shows ventricular fiber orientations on epicardium and endocardium layers from human and a pig hearts and fiber orientations marked on the two-layer LV model corresponding to end-systole and end-diastole conditions [Tang et al., (2008, 2010a,2010b, 2011)].

2.3 A pre-shrink process and geometry-fitting technique for mesh generation.

Under the *in vivo* condition, the ventricles were pressurized and the zero-stress ventricular geometries were not known. In our model construction process, a pre-shrink process was applied to the in vivo end-systolic ventricular geometries to generate the starting shape (zero ventricle pressure) for the computational simulation. Figure 4 shows the no-load LV geometry obtained from the pre-shrink process and the LV geometries with end-systolic and end-diastolic pressure conditions applied, matching in vivo echo geometry data. The initial shrinkage for the short-axis and long-axis directions was 23% and 1%, respectively. Initial shrinkage was needed so that when the end-systolic pressure was applied, the ventricles would regain its *in vivo* morphology. The short-axis shrinkage was larger because the ventricle expanded mostly in the short-axis direction. The outer surface of the ventricular shrinkage was determined by conservation of mass so that the total ventricular wall mass was conserved. Without this shrinking process, if we started from the in vivo end-systolic LV geometry, the ventricle would expand under pressure and its volume would be greater than the acquired in vivo end-systolic ventricle volume leading to large computational errors. The effect of the pre-shrink process will be further demonstrated in Section 3.

A geometry-fitting mesh generation technique we developed in our previous studies was used to generate mesh for our models [Tang et al., (2010a)]. Using this technique, the 3D LV domain was divided into many small "volumes" to curve-fit the irregular ventricle geometry with the infarct tissue as an inclusion. Mesh analysis was performed by decreasing mesh size by 10% (in each dimension) until solution differences were less than 2%. The mesh was then chosen for our simulations.

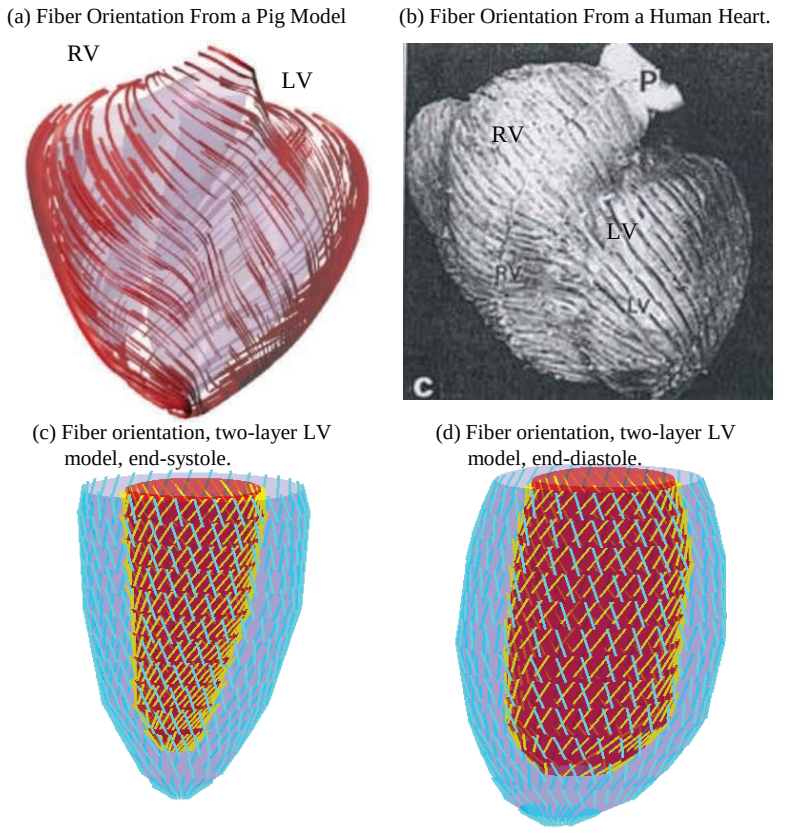

Figure 3: Modeling fiber orientation: (a) Fiber orientation from a pig model; (b) Fiber orientation from a human heart; (c) fiber orientation from our two-layer LV model, end-systolic; (d) end-diastolic condition.

2.4 Solution methods and simulation procedures.

The anisotropic LV computational models were constructed for the 2 patients and the models were solved by ADINA (ADINA R&D, Watertown, MA, USA) using unstructured finite elements and the Newton-Raphson iteration method. Material parameters were adjusted for each patient model to match Echo-measure LV volume data which served as our model validation. Stress/strain distributions were obtained for analysis.

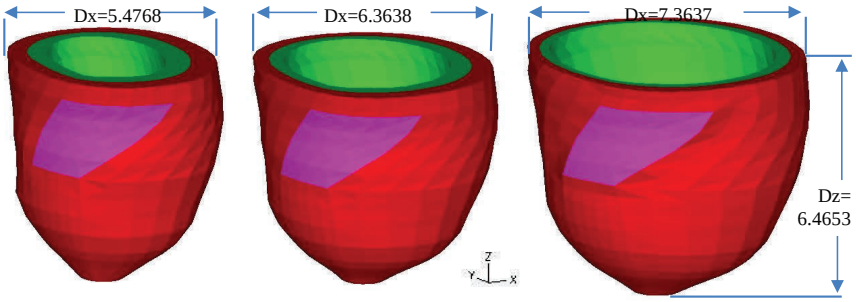

Figure 4: LV geometries corresponding to no-load, end-systolic and end-diastolic pressure condition.

2.5 *Ventricle wall thickness and curvature calculation, data for statistical analysis.*

Patients' end-diastolic LV geometries and stress/strain conditions were used for our comparative study to find out differences between the left ventricles with and without infarct. For each LV data set (P1: 12 slices; P2: 11 slices. Slices are short-axis cross sections), we divided each slice into 4 quarters, each quarter with equal inner wall circumferential length. Ventricle wall thickness, circumferential curvature (C-curvature), longitudinal curvature (L-curvature) and stress/strain were calculated at all nodal points (100 points/slice, 25 points/quarter). Since stress and strain are tensors, the maximum principal stress and strain were used as the representative scalar values for stress and strain at each node, respectively. The "quarter" values of those parameters were obtained by taking averages of those quantities over the 25 points for each quarter and saved for analysis. The quarter values of those from the two patients were compared to see if there are any statistically significant differences. Student t-test was used to compare the data from the two patients.

C-curvature (κ_c) at each point on an RV inner contour was calculated using:

$$\kappa_c = \frac{x'y - xy'}{\left(x'^2 + y'^2\right)^{3/2}} \tag{6}$$

where the contour was a planar curve, x,y are treated as the function of arc, and the derivatives were evaluated using neighboring points on the contour. L-curvature (κ) at each point on an RV inner contour was calculated using:

$$\kappa = \frac{\sqrt{\left(z(t)y'(t) - y(t)z'(t)\right)^2 + \left(x(t)z'(t) - z(t)x'(t)\right)^2 + \left(y(t)x'(t) - x(t)y'(t)\right)^2}}{\left(x'^2(t) + y'^2(t) + z'^2(t)\right)^{3/2}}$$

(7)

where the longitudinal curve is given by **X**=(x(t), y(t), z(t)), the derivatives were evaluated using points from neighboring slices vertically below and above the point being considered.

3 Results

3.1 Echo-based modeling to determine LV tissue material properties

Human ventricle tissue material properties based on in vivo data are extremely hard to get. With patient-specific echo ventricle morphological data and the corresponding pressure conditions, we were able to determine parameter values in the Mooney-Rivlin models in Eq. (3) and (5). Using the fiber coordinates, the strain energy function takes the form (McCulloch):

$$W = \frac{C}{2}\left(e^{Q} - 1\right) \tag{8}$$

$$Q = b_1 E_{ff}^2 + b_2\left(E_{cc}^2 + E_{rr}^2 + E_{rc}^2 + E_{cr}^2\right) + b_3\left(E_{fc}^2 + E_{cf}^2 + E_{rf}^2 + E_{fr}^2\right) \tag{9}$$

The parameter values for the two LVs considered are given in Table 2. Computational volume data matching echo-measured data were provided in Table 1 earlier. Figures 5 gives the stress-stretch ratio plots for the three sets of material curves. It should be noted that it was necessary to adjust the material parameters for the healthy LV to match the volume data, while only one set of material parameters was needed for the patient with infarct. To make the comparison easier, the least-squares method was used to find the equivalent Young's moduli (YM) for all the curves which are given in Table 2. Using the numbers corresponding to the end-diastole condition, the YM value for the fiber direction of LV2 was about 50% stiffer than that of LV1 (108.9 kPa vs. 77.8 kPa). Corresponding to end-systole condition, the YM value for the fiber direction of LV1 was about 100% stiffer than that of LV2 (197.1 kPa vs. 108.9 kPa). The variation of parameters of LV1 indicated that LV1 had more active contraction reflected by material stiffness variations.

3.2 Impact of LV infarct on ventricle morphology and stress distributions.

Comparison of LV quarterly-averaged wall thickness, circumferential and longitudinal curvature, stress and strain values are given in Table 3. Because stress and strain are tensors, maximum principal stress and strain were used as their scalar representatives in this paper. Among the 5 parameters, longitudinal curvature (L-curvature) and LV stress showed the largest differences. At end-systole, L-curvature from LV2 was 164% higher than that from LV1. LV stress from LV2

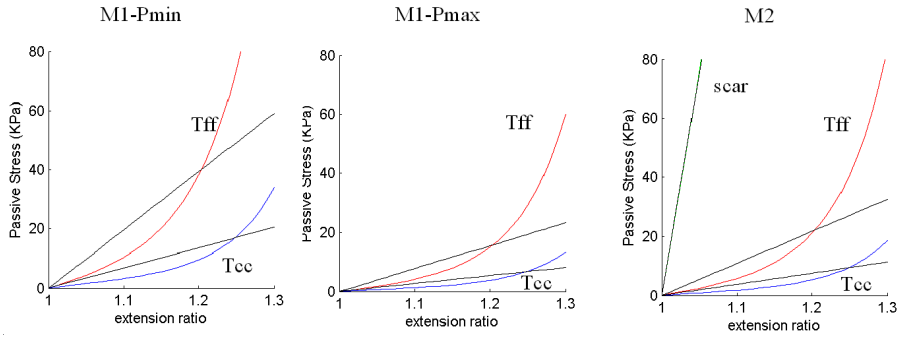

Figure 5: Stress-Stretch plots for the M1 and M2 Mooney-Rivlin models in fiber coordinates. Tff: stress in fiber direction; Tcc: stress in circumferential direction of the fiber. M1: model from the healthy ventricle. M2: ventricle with infarct.

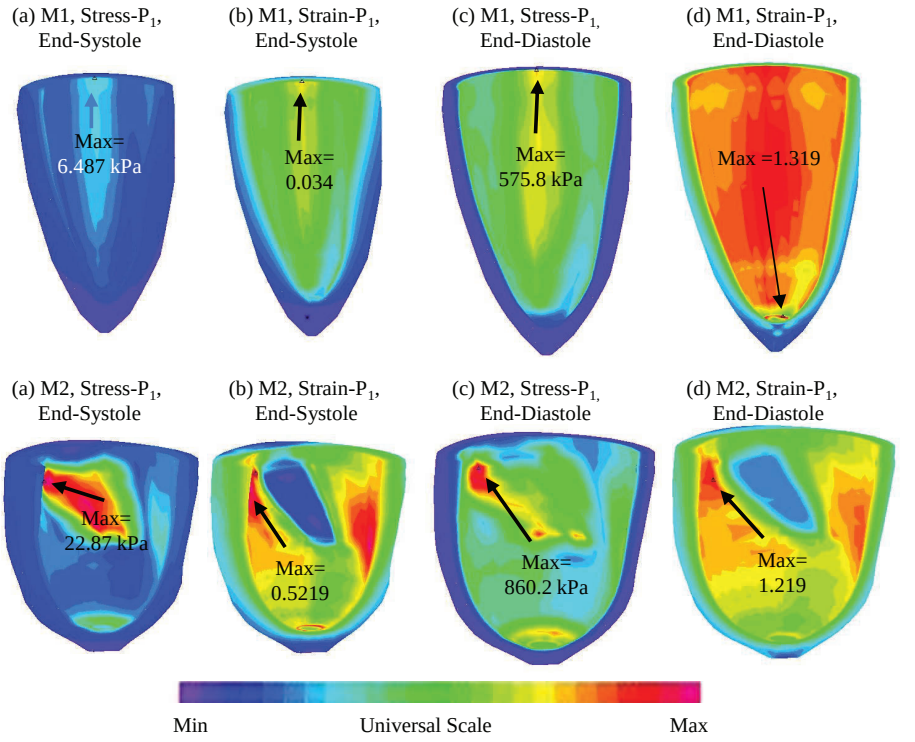

Figure 6: Stress/strain plots, M1: model for healthy LV, M2: model for LV with infarct.

Table 2: Material parameters.

	C(kPa)	b1	b2	b3	Tff YM (kPa)	Tcc YM (kPa)
M1, Pmin	6.8552	8.7875	1.7005	0.7742	197.1	68.2
M1Pmax	2.7060	8.7875	1.7005	0.7742	77.8	26.9
M2	3.7884	8.7875	1.7005	0.7742	108.9	37.7
M2-Scar					1519	

was 82% higher than that from LV1. At end-diastole, L-curvature from LV2 was still 132% higher than that from LV1, while LV stress from LV2 was only 9% higher than that from LV1 with p=0.0878. Differences in LV strain were controversial corresponding to end-diastole and end-systole conditions. Differences in wall thickness and circumferential curvature (C-curvature) were less meaningful.

Figure 6 shows LV stress and strain plots from the two cases corresponding to both end-systole and end-diastole conditions. It is clear that the infarct caused higher stress and strain concentrations, especially at end-systole.

Table 3: Comparison of ventricle wall thickness, circumferential and longitudinal curvature, stress and strain from the two patients. Average quarter values were used in comparison. WT: wall thickness; C-cur: C-curvature; L-cur: L-curvature.

		WT(cm)	C-cur	L-cur	Stress (kPa)	Strain
		End-Diastole				
P1 (Base)	Mean	0.660048	0.643025	0.137181	334.767	1.08055
	Sdv	0.120618	0.4364	0.108408	82.22749	0.10436
P2	Mean	0.7903	0.513895	0.318452	363.9204	0.90530
	Sdv	0.193969	0.344314	0.120578	79.5216	0.15322
	P2/P1	120%	80%	232%	109%	84%
	p(t-test2)	0.000183	0.120866	2.79E-11	0.087847	5.262E-09
		End-Systole				
P1 (Base)	Mean	0.892896	0.954898	0.137994	3.242156	0.212465
	Sdv	0.113271	0.630579	0.137415	0.743194	0.040652
P2	Mean	0.922895	0.658759	0.364602	5.907252	0.33652
	Sdv	0.115765	0.414434	0.195408	2.911361	0.068827
	P2/P1	103%	69%	264%	182%	158%
	p(ttest2)	0.212481	0.009876	4.85E-09	2.28E-08	1.41E-17

3.3 *Effect of infarct and pre-shrink on LV volume and stress/strain distributions.*

The LV with infarct was used to study the effect of infarct and pre-shrink on LV volume and stress/strain distributions. Model 3 (M3) was made by changing the infarct tissue to normal tissue to see what differences it would cause. Model 4 (M4) was made by using the end-systole in vivo geometry of LV2 as the no-load starting geometry of the model to observe the errors one might cause by not employing our pre-shrink technique. Figure 7 gives the volumes curves from M2, M3 and M4. The end-diastole volume of M3 (154.77 ml) was 12.4% higher than that of M2 (137.66), while the end-diastole volume of M4 (231.08 ml) was 67.9% higher than that of M2. Figure 8 presents stress/strain plots from M3 and M4 corresponding to both end-systole and end-diastole conditions. Table 4 summarized the maximum stress/strain values of the 4 models corresponding to both end-systole and end-diastole conditions.

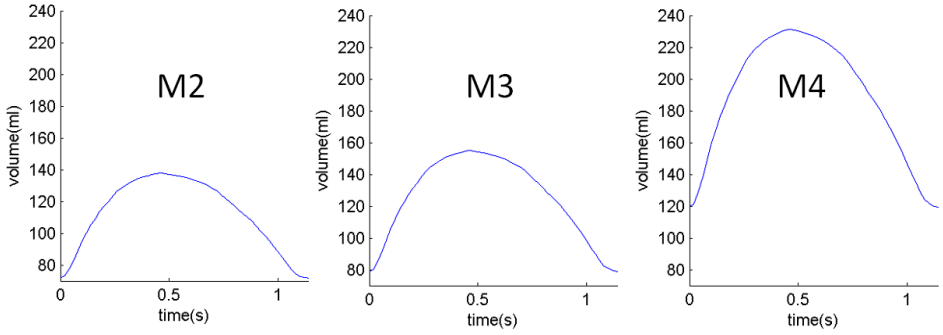

Figure 7: Volume curves from three models.

4 Discussion

This may be the first effort to use echo-based computational modeling approach to investigate left ventricle mechanical stress/strain conditions and identify differences for ventricles with and without infarct. Ventricular morphological and mechanical conditions could serve as the basis for people to develop accurate and automatic methods to identify infarct area based on image data, which is of great clinical relevance. The method presented in this paper serves as the first step. With more patient data and more samples, identification of infarct area could be formulated as an inverse problem and solved numerically. This is closed tied to determination of local ventricle tissue material properties which will require tagging

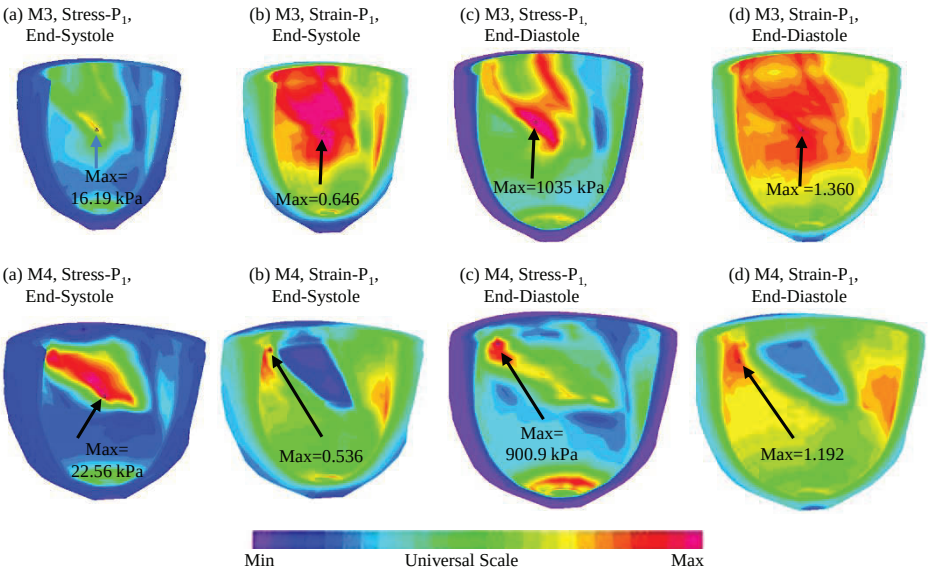

Figure 8: Stress/strain Plots for M3, M4.

Table 4: Comparison of maximum stress and strain values from 4 models corresponding to end-diastolic and end-systolic pressure conditions. M1: healthy ventricle; M2: ventricle with infarct; M3: same as M2 with infarct replaced by normal tissue; M4: model constructed using M2 data without pre-shrink.

	End-Diastole		**End-Systole**	
	Max Stress (kPa)	Max Strain	Max Stress (KPa)	Max Strain
M1	575.8	1.319	6.49	0.3416
M2	861.1	1.219	22.97	0.5224
M3	1035	1.360	16.19	0.6461
M4	900.9	1.192	22.57	0.5358

techniques when LV images were acquired.

Model limitations include the following: a) ventricle valve mechanics was not included. Valve mechanics plays an important role. However, including it will require considerable more data and modeling effort; b) fluid-structure interaction was not included; c) local ventricle deformation imaging data (by particle tracking) was not included; such data will be very useful for determining tissue material properties

and infarct area; d) only passive contraction was modeling in this paper; active contraction by adding active stress and techniques adjusting zero-stress sycamore fiber length could be included in the future.

5 Conclusion

An echo-based computational modeling approach was proposed to investigate left ventricle mechanical properties and stress conditions. With two samples studied, our results indicated that the modeling approach has the potential to be used to determine ventricle material properties. The pre-shrink technique in the model process has considerable effect on model results and stress/strain predictions. Longitudinal curvature and stress showed the largest differences between the two ventricles, with the LV with infarct having higher longitudinal curvature and stress values. More studies are needed to further confirm our findings.

Acknowledgement: This research was supported in part by NIH-1R01-HL 089269 (del Nido, Tang, Geva). Chun Yang's research is supported in part by National Sciences Foundation of China 11171030.

References

Axel, L. (2002): Biomechanical dynamics of the heart with MRI. *Annu. Rev. Biomed. Eng.,* vol. 4, pp. 321-347.

Amundsen, B. H.; Helle-Valle, T.; Edvardsen, T.; Torp, H.; Crosby, J.; Lyseggen, E.; Støylen, A.; Ihlen, H.; Lima, J. A.; Smiseth, O. A.; Slørdahl, S. A. (2006): Noninvasive myocardial strain measurement by speckle tracking echocardiography: validation against sonomicrometry and tagged magnetic resonance imaging. *J Am Coll Cardiol*, vol. 47, pp. 789 –793.

Costa, K. D.; Takayama, Y.; McCulloch, A. D.; Covell, J. W. (1999): Laminar fiber architecture and three-dimensional systolic mechanics in canine ventricular myocardium. *Am J Physiol.* vol. 276, no. 2, H595-607.

Desmond-Hellmann, S.; Sawyers, C. L.; Cox, D. R.; Fraser-Liggett, C.; Galli, S. J.; Goldstein, D. B.; Hunter, D.; Kohane, I. S.; Lo, B.; Misteli, T.; Morrison, S. J.; Nichols, D. G.; Olson, M. V.; Royal, C. D.; Yamamoto, K. R. (2011): *National Research Council (US) Committee on A Framework for Developing a New Taxonomy of Disease. Toward precision medicine: building a knowledge network for biomedical research and a new taxonomy of disease.* The National Academies Press, http://www.nap.edu/catalog.php?record_id=13284

Edvardsen, T.; Gerber, B. L.; Garot, J.; Bluemke, D. A.; Lima, J. A.; Smiseth,

O. A. (2002): Quantitative assessment of intrinsic regional myocardial deformation by Doppler strain rate echocardiography in humans: validation against threedimensional tagged magnetic resonance imaging. *Circulation.* 106:50–56.

Emond, M.; Mock, M. B.; Davis, K. B.; Fisher, L. D.; Holmes, D. R.; Chaitman, B. R. et al.(1994): Long-term survival of medically treated patients in the Coronary Artery Surgery Study (CASS) Registry. *Circulation*, vol. 90, pp. 2645-57.

Gopal, A. S.; Shen, Z.; Sapin, P. M.; Keller, A. M.; Schnellbaecher, M. J.; Leibowitz, D. W. et al. (1995): Assessment of cardiac function by threedimensional echocardiography compared with conventional noninvasive methods. *Circulation,* vol. 92, pp. 842-53.

Guccione, J. M.; Waldman, L. K.; McCulloch, A. D. (1993): Mechanics of active contraction in cardiac muscle: Part II–Cylindrical models of the systolic left ventricle. *J Biomech Eng.*, vol. 115, no. 1, pp. 82-90.

Humphrey, J. D. (2002): *Cardiovascular Solid Mechanics,* Springer-Verlag, New York.

Humphrey, J. D.; Strumpf, R. K.; Yin, F. C. (1999): Biaxial mechanical behavior of excised ventricular epicardium. *Am J Physiol.,* vol. 259, no. 1 Pt 2, H101-8.

Hunter, P. J.; Pullan, A. J.; Smaill, B. H. (2003): Modeling total heart function. *Annu Rev Biomed Eng.,* vol. 5, pp. 147-77.

Kerckhoffs, R. C.; Neal, M. L.; Gu, Q.; Bassingthwaighte, J. B.; Omens, J. H.; McCulloch, A. D. (2007): Coupling of a 3D finite element model of cardiac ventricular mechanics to lumped systems models of the systemic and pulmonic circulation. *Ann Biomed Eng.,* vol. 35, no. 1, pp. 1-18.

Langeland, S.; D'hooge, J.; Wouters, P. F.; Leather, H. A.; Claus, P.; Bijnens, B.; Sutherland, G. R. (2005): Experimental validation of a new ultrasound method for the simultaneous assessment of radial and longitudinal myocardial deformation independent of insonation angle. *Circulation,* vol. 112, pp. 2157–2162.

McCulloch, A. D.; Pfeiffer, E.; Tangney, J.; Omens, J. (2013): Biomechanics of cardiac electromechanical coupling and mechanoelectric feedback. *J Biomech Eng.* doi: 10.1115/1.4026221. [Epub ahead of print]

McCulloch, A. D.; Waldman, L.; Rogers, J.; Guccione, J. M. (1992): Large-scale finite element analysis of the beating heart. *Critical Rev. in Biomed Eng*, vol. 20, no. 5, 6, pp. 427-449.

Mondelli, J. A.; Di Luzio, S.; Nagaraj, A.; Kane, B. J.; Smulevitz, B.; Nagaraj, A. V. et al. (2001): The validation of volumetric real-time 3-dimensional echocardiography for the determination of left ventricular function. *J Am Soc E-*

chocardiogr, vol. 14, pp. 994-1000.

Møller, J. E.; Hillis, G. S.; Oh, J. K.; Reeder, G. S.; Gersh, B. J.; Pellikka, P. A. (2006): Wall motion score index and ejection fraction for risk stratification after acute myocardial infarction. *Am Heart J.,* vol. 151, pp. 419-25.

Nash, M. P.; Hunter, P. J. (2000): Computational Mechanics of the Heart, From tissue structure to ventricular function. *Journal of Elasticity,* vol. 61, pp. 113–141.

Nesser, H. J.; Mor-Avi, V.; Gorissen, W.; Weinert, L.; Steringer-Mascherbauer, R.; Niel, J. et al. (2009): Quantification of left ventricular volumes using three-dimensional echocardiographic speckle tracking: comparison with MRI. *Eur Heart J.,* vol. 30, pp. 1565-73.

Novak, V. P.; Yin, F. C.; Humphrey, J. D. (1994): Regional mechanical properties of passive myocardium. *J. Biomech.* vol. 27, no. 4, pp. 403-12.

Peskin, C. S. (1977): Numerical analysis of blood flow in the heart. *J. Com. Phys,* vol. 25, pp. 220-252.

Peskin, C. S. (1989): A three-dimensional computational method for blood flow in the heart. *J. Comp. Physics,* vol. 81, pp. 372-405.

Quinones, M. A.; Greenberg, B. H.; Kopelen, H. A.; Koilpillai, C.; Limacher, M. C.; Shindler, D. M. et al. (2000): Echocardiographic predictors of clinical outcome in patients with left ventricular dysfunction enrolled in the SOLVD registry and trials: Significance of left ventricular hypertrophy. *J. Am Coll Cardiol,* vol. 35, pp. 1237-44.

Reant, P.; Labrousse, L.; Lafitte, S.; Bordachar, P.; Pillois, X.; Tariosse, L.; Bonoron-Adele, S.; Padois, P.; Deville, C.; Roudaut, R.; Dos Santos, P. (2008): Experimental validation of circumferential, longitudinal, and radial 2-dimensional strain during dobutamine stress echocardiography in ischemic conditions. *J. Am Coll Cardiol.* vol. 51, pp. 149 –157.

Saber, N. R.; Gosman, A. D.; Wood, N. B.; Kilner, P. J.; Charrier, C. L.; Firman, D. N. (2001): Computational flow modeling of the left ventricle based on in vivo MRI data: initial experience. *Annals of Biomech. Engng.,* vol. 29, pp. 275-283.

Sabia, P.; Afrookteh, A.; Touchstone, D. A.; Keller, M. W.; Esquivel, L.; Kaul, S. (1991): Value of regional wall motion abnormality in the emergency room diagnosis of acute myocardial infarction: a prospective study using two dimensional echocardiography. *Circulation,* vol. 84, pp. I85-92.

Sanchez-Quintana, D.; Anderson, R.; Ho, S. Y. (1996): Ventricular myoarchitecture in tetralogy of Fallot. *Heart,* vol. 76, pp. 280-286.

Seo, Y.; Ishizu, T.; Enomoto, Y.; Sugimori, H.; Yamamoto, M.; Machino, T.;

Kawamura, R.; Aonuma, K. (2009): Validation of 3-dimensional speckle tracking imaging to quantify regional myocardial deformation. *Circ Cardiovasc Imaging.* vol. 2, no. 6, pp. 451-9.

Sutherland, G. R.; Di Salvo, G.; Claus, P.; D'hooge, J.; Bijnens, B. (2004): Strain and strain rate imaging: a new clinical approach to quantifying regional myocardial function. *J Am Soc Echocardiogr.* vol. 17, pp. 788–802.

Tang, D.; Yang, C.; Geva, T.; del Nido, P. J. (2010a): Image-Based Patient-Specific Ventricle Models with Fluid-Structure Interaction for Cardiac Function Assessment and Surgical Design Optimization. *Progress in Pediatric Cardiology*, vol. 30, pp. 51-62.

Tang, D.; Yang, C.; Geva, T.; del Nido, P. J. (2008): Patient-specific MRI-based 3D FSI RV/LV/Patch models for pulmonary valve replacement surgery and patch optimization. *J. of Biomech. Engineering*, vol. 130, no. 4, 041010.

Tang, D.; Yang, C.; Geva, T.; Gaudette, G.; del Nido, P. J. (2010b): Effect of Patch Mechanical Properties on Right Ventricle Function Using MRI-Based Two-Layer Anisotropic Models of Human Right and Left Ventricles. *CMES: Computer Modeling in Engineering and Sciences,* vol. 56, no. 2, pp. 113-130.

Tang, D.; Yang, C.; Geva, T.; Gaudette, G.; del Nido, P. J. (2011): Multi-physics MRI-based two-layer fluid-structure interaction anisotropic models of human right and left ventricles with different patch materials: cardiac function assessment and mechanical stress analysis. *Computers & Structures,* vol. 89, pp. 1059-1068.

Thune, J. J.; Kober, L,; Pfeffer, M. A.; Skali, H.; Anavekar, N. S.; Bourgoun, M. et al. (2006): Comparison of regional versus global assessment of left ventricular function in patients with left ventricular dysfunction, heart failure, or both after myocardial infarction: the valsartan in acute myocardial infarction echocardiographic study. *J. Am Soc Echocardiogr,* vol. 19, pp. 1462-5.

Urheim, S.; Edvardsen, T.; Torp, H.; Angelsen, B.; Smiseth, O. A. (2000): Myocardial strain by Doppler echocardiography: validation of a new method to quantify regional myocardial function. *Circulation.* vol. 102, pp. 1158 –1164.